



The Cloud Particle Spectrometer with Polarization Detection (CPSPD): A next generation open-path cloud probe for distinguishing liquid cloud droplets from ice crystals



Darrel Baumgardner^{a,*}, Roy Newton^a, Martina Krämer^b, Jessica Meyer^b, Alexander Beyer^c, Manfred Wendisch^c, Paul Vochezer^d

^a Droplet Measurement Technologies, 2545 Central Ave, Boulder, CO 80301, USA

^b Forschungszentrum Jülich, Institut für Energie- und Klimaforschung Stratosphäre (IEK-7), 52425 Jülich, Germany

^c Universität Leipzig, Leipziger Institut für Meteorologie (LIM), Stephanstr. 3, 04103 Leipzig, Germany

^d Karlsruhe Institute of Technology (KIT), Karlsruhe, Germany

ARTICLE INFO

Article history:

Received 4 March 2013

Received in revised form 13 December 2013

Accepted 16 December 2013

Keywords:

Cloud spectrometer

Liquid/ice discrimination

Ice clouds

Mixed phase clouds

Polarized light

Optical particle counter

ABSTRACT

The differentiation of small water droplets and ice crystals by in situ measurements, in the size range $<50\ \mu\text{m}$, remains a challenge and the lack of such measurements is an obstacle to progress in understanding ice formation in clouds. A new microphysical instrument, the Cloud Particle Spectrometer with Polarization Detection (CPSPD), has been developed that measures light intensity scattered (in forward and backward directions) by individual cloud particles that pass through a focused laser beam and derives their size and thermodynamic phase (liquid or ice) in the optical diameter range from 2 to $50\ \mu\text{m}$. The optical equivalent diameter is derived from the light scattered in the forward direction. The change in polarization state of the incident light, caused by interaction with the cloud particle, is determined from the polarized components of the backscattered light. The CPSPD, along with several other cloud microphysical probes, has been flown on the University of North Dakota Citation aircraft in mixed phase clouds. It has also been deployed and operated at the Zugspitze research station studying mountain clouds. The preliminary results show that liquid cloud droplets can be distinguished from ice crystals and that the ice fraction can be estimated; an important parameter for better understanding of cloud processes, particularly that of glaciation.

© 2013 The Authors. Published by Elsevier B.V. Open access under [CC BY-NC-ND license](https://creativecommons.org/licenses/by-nc-nd/4.0/).

1. Introduction

In spite of the many gains in understanding of cloud processes since Weickman (1945) began collecting ice

crystals from aircraft in the mid 1940s, more than 75 years later there remain serious gaps that limit our ability to predict how clouds precipitate or impact climate. This limitation is partially due to the lack of instruments that can accurately measure the properties of small ice crystals in all-ice clouds, or of small water droplets and ice crystals in mixed phase clouds.

It is known that precipitation will form more rapidly when cloud tops are below the freezing temperature and ice crystals form and grow through a variety of processes, e.g., vapor deposition, riming and aggregation. Numerous theories have been developed that describe the evolution of ice in natural clouds and these processes have been simulated in sophisticated numerical models, yet few measurements have been able to definitively document the environmental conditions under

* Corresponding author. Tel.: +1 303 440 5576.

E-mail addresses: Darrel.baumgardner@gmail.com (D. Baumgardner), newton@dropletmeasurement.com (R. Newton), m.kraemer@fz-juelich.de (M. Krämer), j.meyer@fz-juelich.de (J. Meyer), a.beyer@studserv.uni-leipzig.de (A. Beyer), m.wendisch@uni-leipzig.de (M. Wendisch), paul.vochezer@kit.edu (P. Vochezer).

which these processes occur. Measurements of ice crystal concentrations in cloud, as a function of temperature, frequently exceed by several orders of magnitude what would be predicted from current theories of ice formation so that various secondary ice production mechanisms have been hypothesized. Some of the confusion stems from the lack of ice nuclei (IN) measurements that can capture the possible nucleation modes; however, inadequate instrumentation that can measure the early stages of ice formation also limit our current understanding of ice processes in mixed-phase clouds.

The majority of instruments designed to make airborne measurements in clouds, and currently deployed on research aircraft worldwide, measure cloud particle properties using single particle light scattering or imaging, e.g., see Chapter 5 in [Wendisch and Brenguier \(2013\)](#). Holography is an emerging technology that holds promise for addressing the small particle issue ([Fugal et al., 2004, 2009; Fugal and Shaw, 2009](#)); however, it has a number of its own limitations that will likely limit its broader use for some time to come ([Baumgardner et al., 2011, 2012](#)). The instruments that measure single particle light scattering intensity, e.g. the forward scattering spectrometer probe (FSSP) and the cloud droplet probe (CDP) assume that the particle is a liquid water droplet and derive an optical equivalent diameter using Mie theory ([Mie, 1908](#)). The term “optical equivalent diameter” is used to indicate that the derived particle size is based on the scattering intensity of liquid water droplets of that size. There is no additional information in the scattering intensity by itself; hence, there is no differentiation between liquid water and ice ([Knollenberg, 1976; Baumgardner et al., 2011](#)).

The Small Ice Detector (SID) generates both a particle number size distribution and high resolution scattering patterns of the 5–26° forward scattered light ([Ulanowski et al., 2013; Cotton et al., 2009; Kaye et al., 2008](#)). The scattering patterns of liquid water droplets are Airy disks according to Mie theory. Solid ice particles, however, lead to deviating scattering patterns. Recording the patterns with a high resolution camera enables a sharp discrimination between water droplets and ice particles. It has yet to be demonstrated, however, if recently frozen water droplets can be distinguished from liquid droplets and there are still issues of the maximum concentration of particles that can be measured before coincidence losses become significant ([Johnson et al., in press](#)).

Optical array probes (OAPs) capture the image of a cloud particle by recording with an array of diodes. The minimum resolution that has been successfully realized by an OAP is 10 μm so that the detailed shape of images smaller than about 50–100 μm cannot be recognized given the distortion caused by digitization, i.e. circular images of liquid water droplets cannot be distinguished from frozen droplets or quasi-circular images of ice crystals.

Thus, to measure ice crystal properties in the size range from approximately 1 to 50 μm remains a challenge, even though there are several promising technologies that are still evolving. One such new technology is the Cloud Particle Spectrometer with Polarization Detection (CPSPD), a modification to the single particle light scattering technique, that uses the change in polarization state of scattered light to separate liquid water droplets from ice. The CPSPD is the next generation version of the Cloud and Aerosol Spectrometer

with Polarization (CAS-POL, [Glen and Brooks, 2013](#)). Here we describe the measurement principles and show preliminary results from samples taken in mixed phase clouds. We emphasize at this point that the primary objective of this paper is to introduce a new a technology that is still evolving; hence, the focus is more on methodology than on science, although preliminary results will be shown that illustrate the potential of the CPSPD to make a significant contribution to the science of ice in clouds.

2. Measurement technique

2.1. Basic principles

The CPSPD employs single particle light scattering as its measurement methodology. Unlike the FSSP ([Knollenberg, 1976; Wendisch et al., 1996](#)) or CDP ([Lance et al., 2010](#)), that collect light over a solid angle between nominally 4° and 12°, the CPSPD collects light from two separate collection angles, forward and backward, similar to what is done in the Cloud Aerosol and Spectrometer (CAS) ([Baumgardner et al., 2001](#)). The two different scattering angles were implemented to detect the asphericity of particles, since the relationship of forward to backward scattering is dependent on the size, refractive index and shape of the particles ([Baumgardner et al., 2005](#)). The CAS was modified in 2010 to measure the change in the polarization state of the incident laser caused by particles ([Glen and Brooks, 2013](#)). This addition to the CAS, modifying it to the CAS-POL, was made because of the ambiguities in scattering intensity that result from the non-monotonic relationship between particle size and scattered intensity, i.e. different particle sizes can scatter the same intensity of light in the forward and backward directions. This limits the use of multiple angle data to a few selected size ranges.

The polarization component of incident and scattered lights contains additional information on the particle shape as well as its internal structure. For a detailed, theoretical discussion of how particles interact with electromagnetic radiation, the reader is referred to the seminal work of [Bohren and Huffman \(1983\)](#), particularly the first two chapters for explicit description of the interaction between incident light and an individual particle. The central point is that the interaction of a particle with incident, polarized light will produce scattered light whose polarization state will no longer be identical to that of the incoming light. The degree that this state of polarization is changed depends on the particle properties, i.e. the size, morphology and refractive index, and on the angle with respect to the incident radiation that the scattering is viewed. [Fig. 1](#) shows a conceptual illustration of how spherical particles interact with polarized light compared to aspherical particles. In general, spherical particles will change the polarization state only a small amount but not as much as particles with more complex morphology. Frozen water droplets, although spherical, will change the polarization state because of their crystalline structure. Hence, adding a measurement of the polarization state of scattered light complements the multi-angle method for identifying aspherical cloud particles that are presumably ice (although there is also the potential for interference from dust particles).

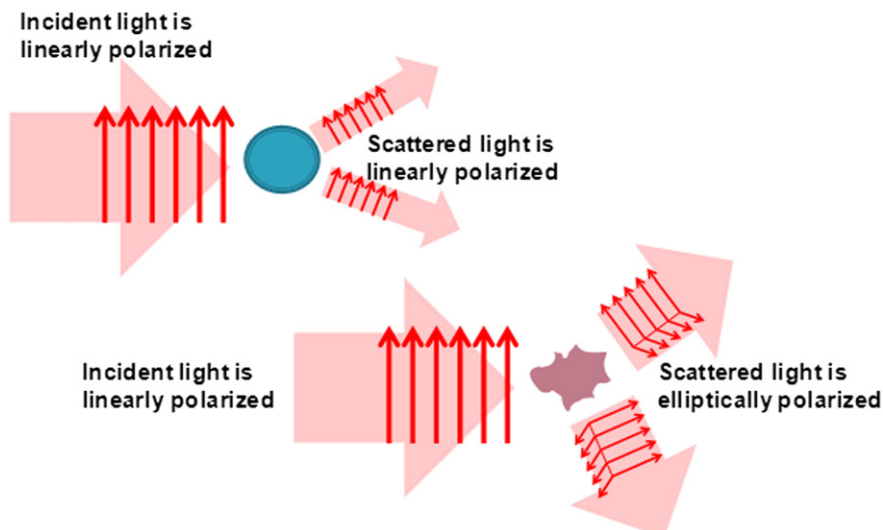


Fig. 1. Conceptual diagram illustrating the interaction between linearly polarized light and spherical and aspherical particles. Spherical particle, in general, will scatter light that is in the same plane of polarization as the incident light. Aspherical particles will scatter light whose polarization is partially in the same plane of polarization as the incident light while some fraction will be in the plane perpendicular. Hence, the resulting scattered light can be considered elliptically polarized.

The use of polarization measurements to distinguish liquid water droplets from ice particles has been used in the past. Fukuta and Kramer (1968) employed a detector in an ice nuclei counter to separate liquid water droplets from activated IN in laboratory studies. The first airborne instrument using polarization was developed at the University of Washington (Turner and Radke, 1973) and was used to detect ice crystals larger than about 150 μm . In the late 1970s, a detector was added to a two-dimensional OAP to measure polarized, scattered light (Knollenberg, 1981; Harris-Hobbs and Cooper, 1987). It was also only effective in detecting ice particles larger than about 90 μm .

There was a lapse in activity related to the use of in-situ polarization measurements or the development of any new sensors after about 1983 (no information is available on which 2D probes had the polarization option or who has made measurements with it other than those published by Harris-Hobbs and Cooper, 1987). More than two decades passed before Nicolet et al. (2007) published theoretical results of modeling the scattering by columnar ice crystals of polarized light in preparation for building a detector measuring circularly polarized light in an IN counter, similar to what Fukuta and Kramer had done almost 40 years earlier. In 2008, Bundke et al. (2008) published results from a new IN counter that also used a detector to measure polarized light. This was closely followed by results published by Nicolet et al. (2010) from their IN counter.

Polarization measurements for the remote sensing (active and passive) of ensembles of particles have been in use for many years with radar and lidar being the best examples of how detection of the change in polarization state is a clear indicator, not only of the water phase of particles, but also of their orientation as well. Indeed, the measurement of changes of liquid water droplets to ice crystal is made in the Aerosol Interaction and Dynamics in the Atmosphere (AIDA) cloud chamber using a measurement of backscattered, polarized light from ensembles of particles (Schnaiter et al., 2012).

The polarization technique is implemented in the CPSPD as shown in Fig. 2, a schematic with the basic optical components to show the forward and backward paths of the scattered light, the forward scattering sizing and qualifier detectors and the “S” and “P” backscattering detectors. The forward scattered light is collected over a cone defined by the collimating optics with angles from 8° to 34°, focused on a beam splitter that directs 70% of the light to a “qualifier” detector masked with a slit aperture and the remaining 30% to a “sizer” detector. The slit aperture constrains the scattered light reaching the qualifier to a region of about 0.5 mm either side of the center of focus, defined as the depth of field (DOF), so that any particles, whose signals measured with the qualifier are less than those from the sizer, will be rejected as out of focus. This aperture also constrains particles by rejecting those that pass through the less intense edges of the laser beam that has a Gaussian intensity profile. This width, defined as the effective beam diameter (EBD), is about 0.12 mm. This constrains particles, regardless of their size, to pass within the $\pm 5\%$ of the most intense region of the beam. The sample area, defined as the DOF \cdot EBD, is 0.12 mm^2 . This sample area not only is sufficiently small to minimize coincidence losses but also impacts sampling statistics.

A particle's equivalent optical diameter (EOD) is derived from the scattering intensity by calibration and Mie scattering theory. Spherical polystyrene latex (PSL) and crown glass beads, both with known refractive indices, are used to relate the scattering intensity measured at a detector to a known particle optical cross section. The EOD is then derived by assuming that the particles are spherical and have a refractive index of liquid water (1.33) at the wavelength of the laser diode (685 nm). Although the EOD is only physically relevant when the particle is actually a liquid water droplet, the EOD is very relevant with respect to the optical properties of the particle, i.e. for the purposes of understanding how an ice crystal interacts with solar

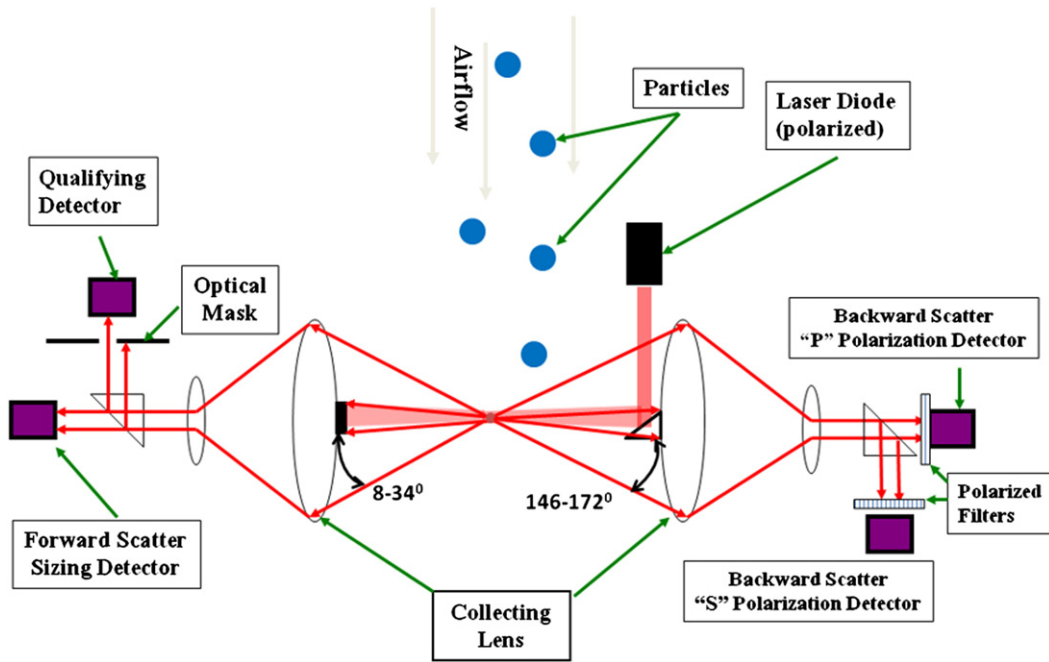


Fig. 2. This diagram shows the principal optical components, and the optical path of scattered light, for the CPSPD.

radiation, the EOD can be used to estimate parameters like the extinction coefficient and optical depth without knowing the actual shape of the particle. This only accounts for the forward

scattering component of a particle, however, and the backscattering intensity is needed to estimate the amount of light returned in the back hemisphere.

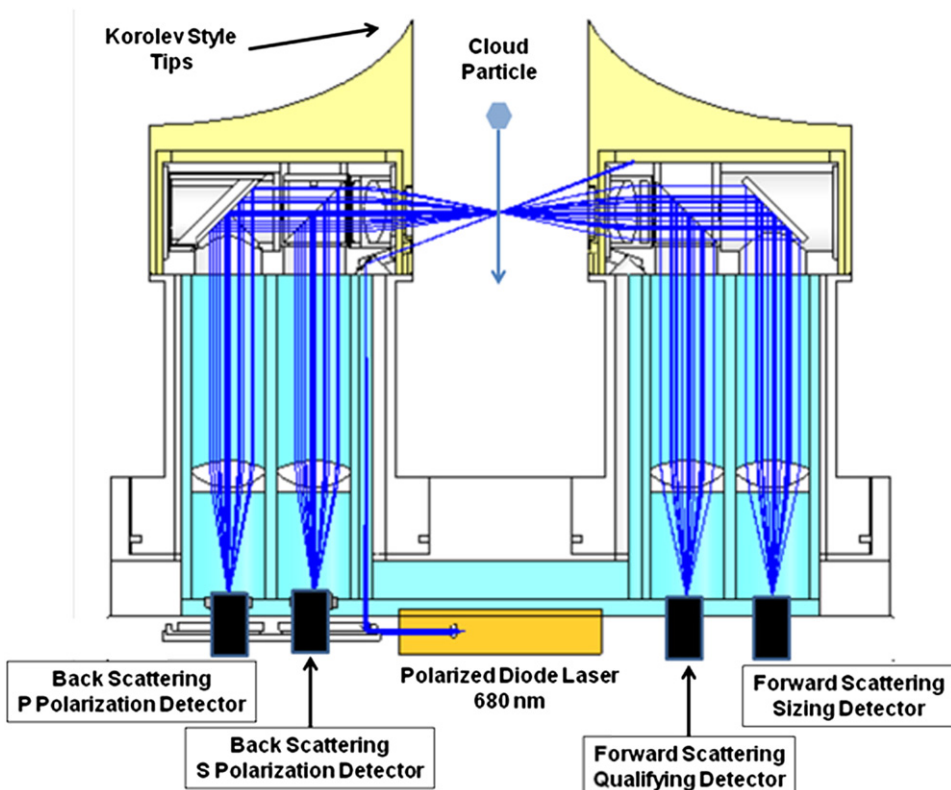


Fig. 3. This diagram shows the layout of the optical components in the CPSPD mechanical housing.

The two back detectors measure the scattered light within a cone defined by the angles 146° – 172° . A polarizing beam splitter separates the backscattered light into components that are parallel (P) and perpendicular (S) to the polarization of the incident light. Hence, the three signals that are analyzed to differentiate particle morphology are the forward scattered and the “P” and “S” back scattered light. Fig. 3 shows the actual, mechanical/optical implementation of the diagram shown in Fig. 2.

The three scattering signals from the detectors in the CPSPD are digitized after which the processing electronics detect the maximum values for each particle that is qualified, i.e. within the DOF and the EBD. A size histogram is accumulated each second by using a look-up table that relates the amplitude of the forward scattering signal to the EOD. The nominal size range from 2 to $50\ \mu\text{m}$ is divided into 30 equal-width intervals and the channel corresponding to the EOD of each particle is incremented by one. This histogram is transmitted to the data system each second. An additional set of information for each particle is also transmitted each second. The digitized values of the forward, S and P

scattering signals are recorded for each particle, along with their transit time (TT) and interarrival time (IAT).

The TT is the duration of the particle while it is in the sensitive sample volume and is recorded from the time the forward scattering signal exceeds the noise level in the electronics until it falls back below this level. The TT is a function of the aircraft velocity and the EOD. For a constant airspeed, larger particles will have longer TT since they will exceed the noise level sooner than smaller particles and remain above this level longer. Fig. 4a is a frequency histogram of TT over one entire research flight of the citation (discussed in Section 3.1). The range of TT in this figure is a result of airspeeds between 80 and $110\ \text{ms}^{-1}$.

The IAT is the measure of how much time has passed since the previous particle left the beam. This parameter is useful for examining the detailed structure of a cloud (Baumgardner, 1986) and also as a means to detect particles that might be a result of shattering (Field et al., 2003, 2006). The spacing between cloud particles can be predicted with Poisson statistics if the particles are assumed distributed uniformly random in space. Fig. 4b shows a frequency distribution of the IATs

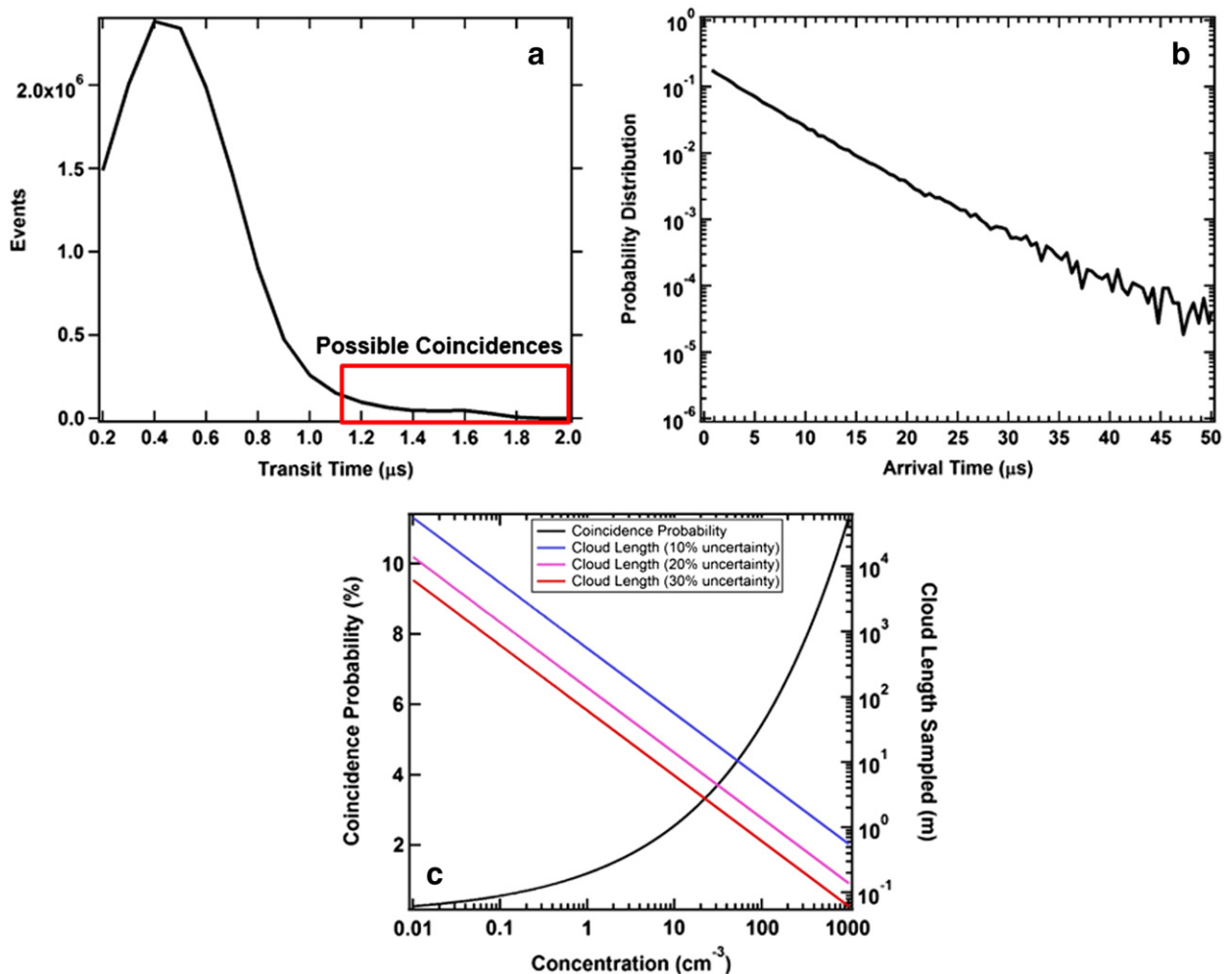


Fig. 4. Shown here are the frequency distributions of transit times (a) and interarrival times (b) of cloud particles during one cloud pass. The probability of coincidence particles (black curve) is drawn in (c) along with the lengths of cloud that would need to be measured for sampling uncertainties of 10% (blue), 20% (magenta) and 30% (red).

measured during one of the cloud passes discussed in Section 3.1. This is a cloud pass with moderately high concentration of particles and the OAP that measures images in the range of 25–3200 μm also showed the presence of ice crystals; hence, it is likely that the potential of ice crystal shattering existed. The so-called “Korolev tips” (Korolev et al., 2013) on the arms of the CPSPD are designed to direct the fragments of shattered ice particles away from the sample volume; otherwise the fragments would pass through in a cluster leading to an increased number of events at very short IATs (Field et al., 2003, 2006). Without the presence of shattering, the frequency distribution of IATs, plotted on a log–log chart, will be a straight line since the probability that an IAT = t is an exponential distribution whose expected value is only a function of the average particle concentration. As seen in Fig. 4b, the frequency distribution, plotted on a log–log scale, is linear with no evidence of an enhanced number of events at the small IATs; hence, any shattering on the arms is contributing negligibly to the number concentration of the particles.

Multiple particles, coincident in the sample volume, cause a measurement uncertainty that needs to be minimized and corrected (Baumgardner et al., 1985). This is normally a problem only when the concentration exceeds about 500 cm^{-3} ; but the probability of occurrence can be estimated based on the number concentration and the size of the active sample volume of the CPSPD. The probability that a particle will enter the active area of the CPSPD before the previous particle has exited is $P(x < \text{EBD}) = 1 - \exp(-x/d)$, where x is the distance between particles and d is the average distance between cloud particles, $d = C^{-1/3}$, where C is the number concentration. The black curve in Fig. 4c shows the probability of a coincidence event as a function of the concentration. At the maximum number concentrations discussed in Section 3.1, 200–300 cm^{-3} , approximately 7% of the particles are undetected due to coincidence.

One of the indications of coincidence is a measured TT larger than the average, since the two or more particles in the beam will appear as one but with an extended TT. In the frequency distribution of TT shown in Fig. 4a, there are TTs larger than 1 μs that are likely a result of coincidences. At the moment we do not use TT to filter these particles but analysis algorithms are under development that will include this as part of the processing.

Also shown on Fig. 4c are the distances through cloud that need to be measured in order to obtain statistically significant samples. Again returning to Poisson statistics, assuming uniformly random spacing of the particles in the cloud, the binomial sampling theorem states that the probability with which a sample represents the local population is equal to $n^{-1/2}$ where n is the number of particles detected. Hence, to insure that there is $\leq 10\%$ error in sampling, at least 100 particles must be detected. The number of particles detected by the CPSPD = $C * \text{EBD} * \text{DOF} * L$, where L is the distance through cloud. In Fig. 4c, the blue, magenta and red curves are for sampling errors 10%, 20% and 30%, respectively. Hence, for typical cloud concentrations of 10–500 cm^{-3} , a representative sample can be taken within less than 10 m. When analyzing concentrations by size, however, where the concentration per size interval will be much less, especially for larger particles, a much longer distance through cloud must be sampled, up to

10 km when the concentration is as small as 0.01 cm^{-3} (Fig. 4c) even when accepting an uncertainty of 20%.

Fig. 5 is a photo of a CPSPD mounted on one of the aircraft wing pylons. In this photo we see one of the primary advantages of the CPSPD over the current CAS-POL design (Glen and Brooks, 2013). The CAS-POL has an inlet that is subject to effects of ice crystal shattering, discussed above (Field et al., 2003, 2006). The CPSPD utilizes the “Korolev” design (Korolev et al., 2013) that directs such shattered fragments outward and away from between the arms.

2.2. Theoretical studies

The relationship between the interaction of light and a particle is complex and depends on the wavelength of incident light, the physical–chemical properties of the particle, i.e. size, refractive index and shape, and its orientation with respect to the incident light. The scattering cross sections of spherical particles can be calculated with knowledge of the wavelength and refractive index, depending on the size of the particle with respect to the wavelength of light. Similar calculations are possible for aspherical particles using a number of different approaches like T-matrix, ray tracing or discrete dipole moments, and assuming a specific non-spherical shape for the particle.

In order to assess the potential response of the CPSPD to non-spherical particles, we took a simplistic approach using oblate and prolate spheroids with a range of EODs and aspect ratios (maximum length to maximum width). We used the open source code of Mishchenko (2000) for deriving the scattering cross section as a function of the angle of the spheroid with respect to the incident light, the aspect ratio and the effective size (volume equivalent diameter) with the



Fig. 5. This is a photo of the CPSPD mounted on an aircraft wing pylon.

methodology called “T-matrix”. Similar to the studies of Nicolet et al. (2012) we calculated solutions for a range of EODs from 1 to 16 μm , aspect ratios from 0.1 to 1.9 and orientation angles from 0 to 180° around the azimuth and from 0 to 360° around the zenith with respect to the incident light. Fig. 6 illustrates the coordinate system and rotational angles. The range of effective diameters was limited by the precision and computational power. The T-matrix method requires extensive calculations and fails to reach convergence beyond a certain size parameter that is dependent on the maximum wavelength of the selected computer. Although cloud particles clearly grow to much larger sizes, the objective of the calculation was to assess the range of polarization ratios, defined here as $\delta = (S - P) / (P + S)$, where S and P are the parallel and perpendicular components, respectively of the scattered light.

Fig. 7 illustrates the results from these calculations for one effective size (2 μm) and aspect (0.9) ratio, over 2592 orientation angles for the backscattering collection angles of the CPSPD. There is a range of angles whereby this ratio reaches maximum and minimum values. The maxima are reached when the largest geometric cross section is presented to the incident laser beam and the minima are when the smallest cross section is viewed with respect to the incident laser. These two regions represent about 25% of all the possible orientations so that for this effective diameter and aspect ratio, the average δ is $0.18 \pm 25\%$. Even in a completely glaciated ice cloud, this technique may identify some fraction of the particles as liquid water droplets based on the polarization signals alone.

Fig. 8 shows a more comprehensive summary of the T-matrix calculations, plotting the average δ as a function of the effective diameter. The number at each marker represents the aspect ratio at that size and δ . In this figure no obvious trend in the δ with either equivalent diameter or aspect ratio is noted. The reason for this variability is related to the complex relationship between the incident light and the particle shape, size and orientation. Although not intuitively obvious, it means that some

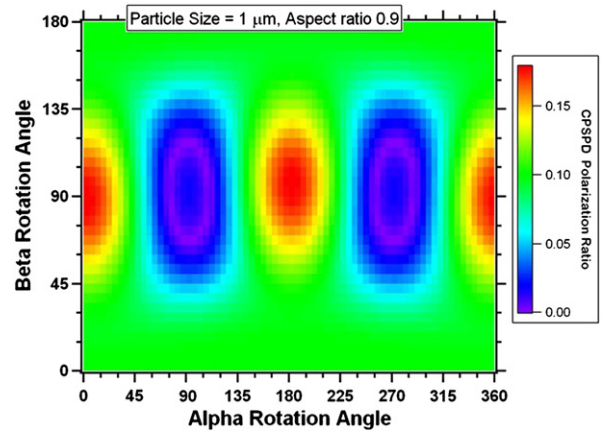


Fig. 7. This contour map of the CPSPD polarization ratio, $S / (S + P)$, shows the sensitivity of this ratio to the orientation of the particle with respect to the incident light. This example is for a small oblate spheroid with a diameter of 1 μm and aspect ratio of 0.9. The pattern of the polarization ratio changes as a function of particle size and aspect ratio.

fraction of recently frozen water droplets, that are quasi-spherical, i.e. with aspect ratios close to 1, should be detectable as ice and not liquid water droplets.

In Figs. 7 and 8, δ is used as an indicator of aspherical particles. δ , as defined here, is one form of the metric that is commonly used by the lidar community as an indicator to separate liquid water droplets from ice crystals or to identify layers of dust or volcanic ash. This metric is used by that community since they only have S and P polarized backscattered signals to work with that are measured from ensembles of particles. Hence, the δ they derive is an average over a large number of sizes, shapes and orientations. On a single particle basis, the δ measured by the CPSPD will have a much larger deviation, as will be observed in the results from Section 3.1.

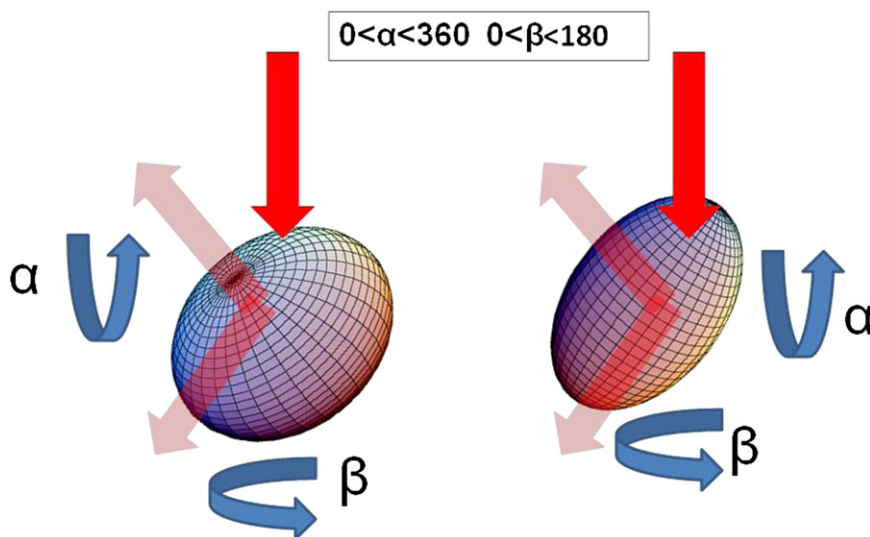


Fig. 6. The T-matrix, light scattering calculations were made on individual particles represented by oblate (left) and prolate (right) spheroids, oriented with respect to the incident light (red arrows) over the full range of possible azimuthal (β) and zenith (α) angles.

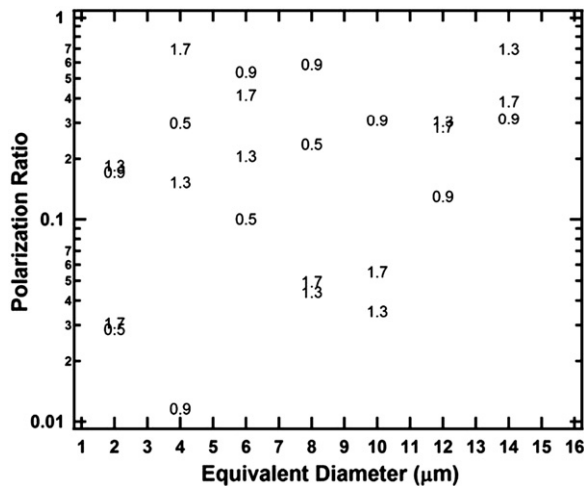


Fig. 8. As illustrated in this figure, the average polarization ratio does not change in a systematic way with aspect ratio or equivalent optical diameter (EOD). These data were generated from the T-matrix calculations where the polarization ratio is the average over all 2592 orientations.

With the CPSPD the forward scattering signal also is available to evaluate particle properties, i.e. their EOD. Whereas the forward scattering signal can directly be related to an EOD, a reference particle that can be used to calibrate the polarized detectors has yet to be found. Hence, the δ is, for the moment, a relative parameter with arbitrary units. As discussed below, until we can find a good reference particle with known properties as they relate to the change in polarization of incident light, the results will be discussed in terms of relative rather than absolute magnitudes.

3. Results from measurements in natural clouds

3.1. Airborne measurements

The CPSPD was mounted on the University of North Dakota Cessna Citation jet aircraft in the autumn of 2011 to take part in an instrumentation comparison project. The aircraft is equipped with a CDP and 2D-OAP (25–800 μm) as well as the standard suite of sensors for measuring winds and state parameters. A number of new instruments, including the CPSPD, were flown in mixed phase clouds to compare with the conventional cloud probes. Rather than investigating any specific cloud microphysical process, this project was dedicated to probe evaluation, particularly under conditions of super-cooled liquid droplets mixed with ice crystals,

The ice fraction in clouds is computed from the particle by particle δ values computed from the S and P signals. Fig. 9 shows the δ values, averaged every 5 s, for one entire flight, as a function of the median volume diameter and temperature (color coded on the markers). Unlike the simulated δ values shown in Fig. 8, calculated from theoretical values of S and P, the measured S and P are, at the moment, uncalibrated so that the δ derived from the observations cannot be directly related to the theoretical values. It is noted, however, that the observed δ values have a similar range as those that were

simulated. In order to compute an ice fraction, a threshold value for the δ was selected as the separation between a spherical liquid water droplet and aspherical ice crystal. There were only two flights during this project, neither of which were flown through pure liquid water clouds, so there are not any δ values that can be definitely related to spheres; however, given the temperature range where data was taken in clouds, $-1\text{ }^\circ\text{C}$ to $-8\text{ }^\circ\text{C}$, it is reasonable to assume that these were mixed phase clouds and that the δ for water droplets seems to fall between 0.4 and 0.55 (Fig. 9). A value of 0.6 was taken as a threshold above which a particle was considered as ice.

Fig. 10 shows time series from measurements made on November 11, 2011, through a number of clouds over the time period from 1600 to 1800 UTC. Total number concentrations are drawn in Fig. 10a as measured with the CPSPD (black) and CDP (blue), as well as those derived from the CPSPD as being only ice (black dotted). The CPSPD and CDP are generally in good agreement with occasional deviations, especially during the second half of the flight. It is interesting to note that, whereas the total concentration from the CPSPD remains fairly constant from 60600 s to 63000 s, the ice concentrations tends to follow the same trend as the CDP.

The liquid water content (LWC) and median volume diameters (MVDs) from the CPSPD and CDP are compared in Fig. 10b. As with the number concentrations, the agreement is generally good, although the CPSPD MVD is constantly higher than the CDP by about 5 μm until 60600 s at which point the two probes converge. The two time periods where the CDP abruptly increases above the CPSPD, 59900 s and 60200 s, do not show similar variations in either the number concentration or the MVD. It should be noted that the CPSPD was located on the right wingtip whereas the CDP was on the left wingtip. This is a distance of approximately 13 m, so that the two probes would not be expected to be perfectly correlated due to the natural variations in cloud properties.

Fig. 10c shows the trends in the ambient temperature and ice fraction with time. The color shading on the ice fraction curve is related to the MVD. From 59400 s to 60100 s the temperature is decreasing and the ice fraction increases. This is especially noticeable when the temperature decreases 2 $^\circ\text{C}$ at 59900 s and the ice fraction increases at the same time. During all the periods with ice fraction greater than about 0.05, the 2D-OAP was also registering ice particles, as shown by one representative strip at the bottom of the figure and related to the period surrounded by the red box. These are much larger ice particles than can be measured by the CPSPD, ranging from 200 to 400 μm in maximum diameter for the particular example; however, it lends support to the contention that the CPSPD is indeed detecting ice among the water droplets.

Fig. 11 is a contoured time series where the color coding represents the ice fraction as a function of EOD. Also shown is the temperature (black curve). The blue box highlights a region where the ice fraction is increasing with decreasing diameter. This is indicated by the sloping downward of the red, yellow and green regions, i.e. moving towards smaller diameters as the temperature decreases. This figure shows that nearly all of the particles $>35\text{ }\mu\text{m}$ are ice while the majority of particles $<15\text{ }\mu\text{m}$ are droplets. This tendency for larger liquid water droplets to freeze before the smaller ones has been demonstrated in the laboratory (Gonda and

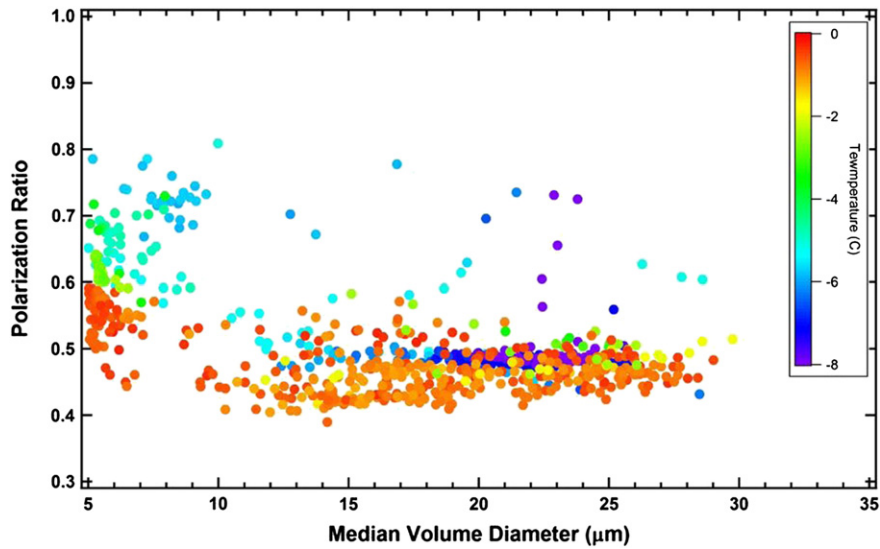


Fig. 9. The polarization ratio, δ , averaged every 5 s during the five cloud passes of the research flight, are shown here as a function of the averaged median volume diameter and temperature (color coded).

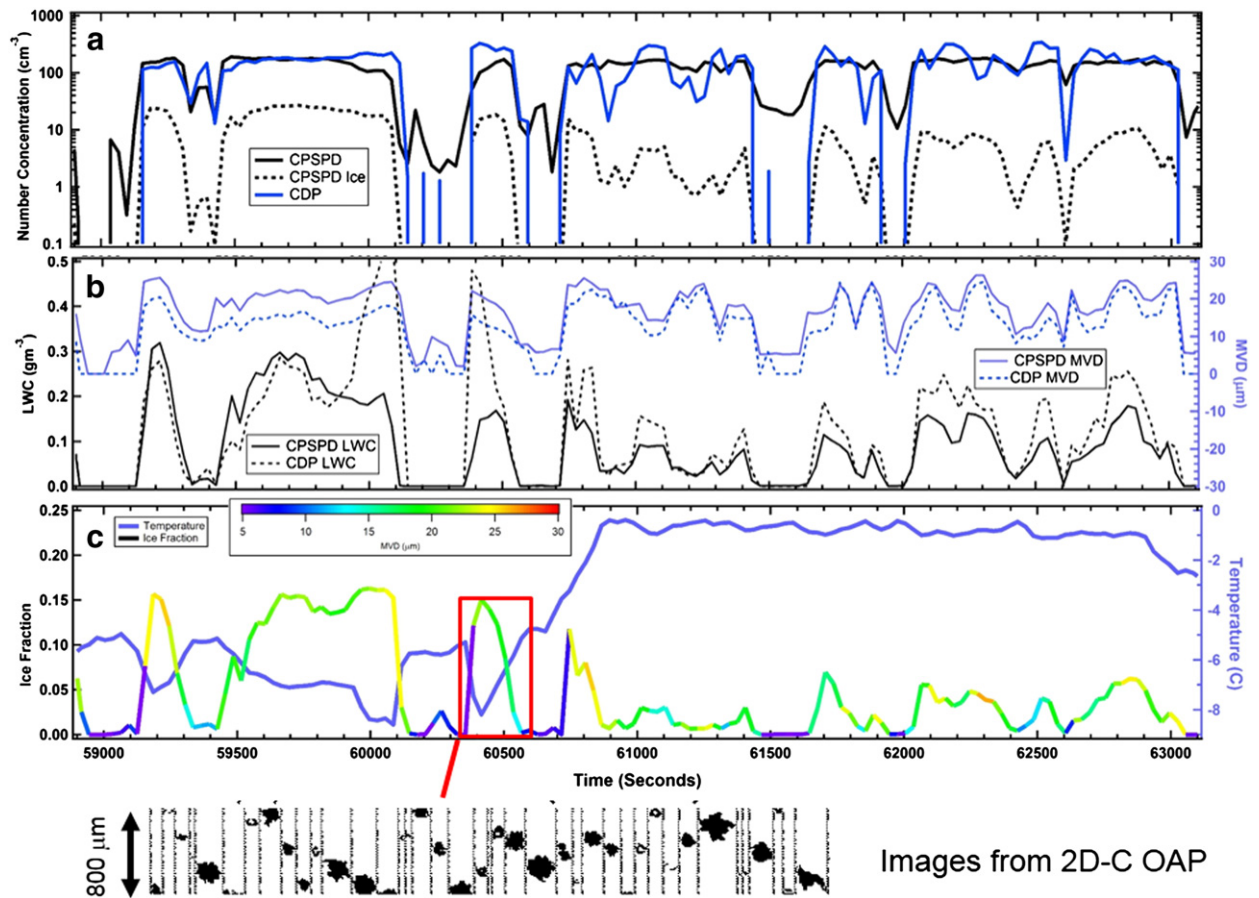


Fig. 10. These time series show (a) the number concentrations from the CPSPD (black solid), CDP (blue) and ice concentration from the CPSPD (black dotted), (b) LWC from the CPSPD (black solid) and CDP (black dotted) and MVD from the CPSPD (blue solid) and CDP (blue dotted), and (c) the ice fraction derived from the CPSPD (colored by MVD) and the temperature (blue). Also shown are images from the 2-D optical array probe (OAP) for the period within the red box.

Yamazaki, 1984) and in natural clouds (Korolev and Isaac, 2003). There are clear trends in the ice fraction patterns and the temperature such as at 60300 s when the temperature increases and the ice fraction between 0.2 and 0.4 (light blue) moves from 18 μm to 22 μm , i.e. fewer of the larger particles are ice as the temperature increases.

3.2. Mountaintop measurements

In September, 2012 the CPSPD was mounted at the mountaintop laboratory of the environmental research station Schneefernerhaus (Umwelt Forschungsstation Schneefernerhaus, UFS, <http://www.schneefernerhaus.de/>) on Mount Zugspitze (47.4°N, 11°E, 2962 m a.s.l.) as part of a project to study cloud formation and evolution (ACRIDICON Zugspitze). Since the CPSPD is designed for airborne operations, a special system was designed to aspirate it. The arms were enclosed with a chamber that surrounds the sample volume of the probe and a vacuum system was attached via a flexible hose to maintain flow through the arms at a constant, controlled rate. Besides the CPSPD was the mounted Particle Phase discriminator version two, Karlsruhe edition (PPD2-K,). The PPD2-K is an instrument from the small ice detector (SID) family of instruments mentioned above. The PPD2-K is designed for stationary measurements and its measurement results are equivalent to the SID3. (Kaye et al., 2008).

The CPSPD was operated from September 17 to October 2, sampling a variety of clear air and cloudy conditions. Fig. 12 illustrates one of the periods, September 27, when a cloud was present with temperatures just below freezing, -2°C to -4°C . There were problems with the PPD2-K data acquisition software on the 27th and thus the available PPD2-K data is limited to the period 18:00–19:15 UTC. In Fig. 12a and c we show that the total number concentration and ice fraction vary quite a lot, from 0.1 to 100 cm^{-3} and 0.0 to 0.07, respectively. The size distribution, as a function of time, shown in Fig. 12b has a broad peak

between 8 and 20 μm early in the period but the peak narrows to 20 μm later in the time period. The size distribution of the ice fraction, shown in Fig. 12d shows that the highest ice fractions, between 0.5 and 0.6 are at the largest sizes, decreasing with decreasing diameter, similar to what was seen with the aircraft observations.

The PPD2-K observations between 18:00 and 19:15 UTC, corresponding to the CPSPD measurements shown in Fig. 12, are illustrated in Fig. 13. It is noted here that the size range of the PPD2-K, 7 to 100 μm , is different than the 2–50 μm range of the CPSPD. As seen from the CPSPD size distributions in Fig. 12b, particles less than about 5 μm have concentrations between 10 and 50 cm^{-3} ; hence, the total concentrations measured by the CPSPD are expected to be greater than those measured with the PPD2-K. There are however, some general trends seen in the measurements from both instruments. The period from 18:45 to 19:15 has several features that are particularly noteworthy. In this time period the concentrations are observed to decrease with most of the decrease coming from particles in the size range between approximately 5 and 10 μm , as can be in Figs. 12b and 13b. The size distributions from both instruments are also bimodal. The CPSPD size distribution shows peaks at 3 μm and 10 μm and the PPD2-K has modes at approximately 8 and 20 μm .

The ice fraction from the CPSPD (Fig. 12c) reaches its maximum value during the time period 18:45 to 19:15 when the size distribution becomes bi-modal and the number concentration is at a minimum. Likewise, the ice fraction from the PPD2-K, derived by analyzing the forward scattering patterns (Kaye et al., 2008; Cotton et al., 2009), is a maximum over this same time period (Fig. 13c). Fig. 13d indicates that larger particles are almost exclusively ice which is in accordance with the trends seen in the CPSPD measurements (Fig. 12d). Furthermore Figs. 12d and 13d indicate that the occurrence of small and large ice particles is highly correlated. Overall the results from the CPSPD and PPD2-K are in reasonable agreement.

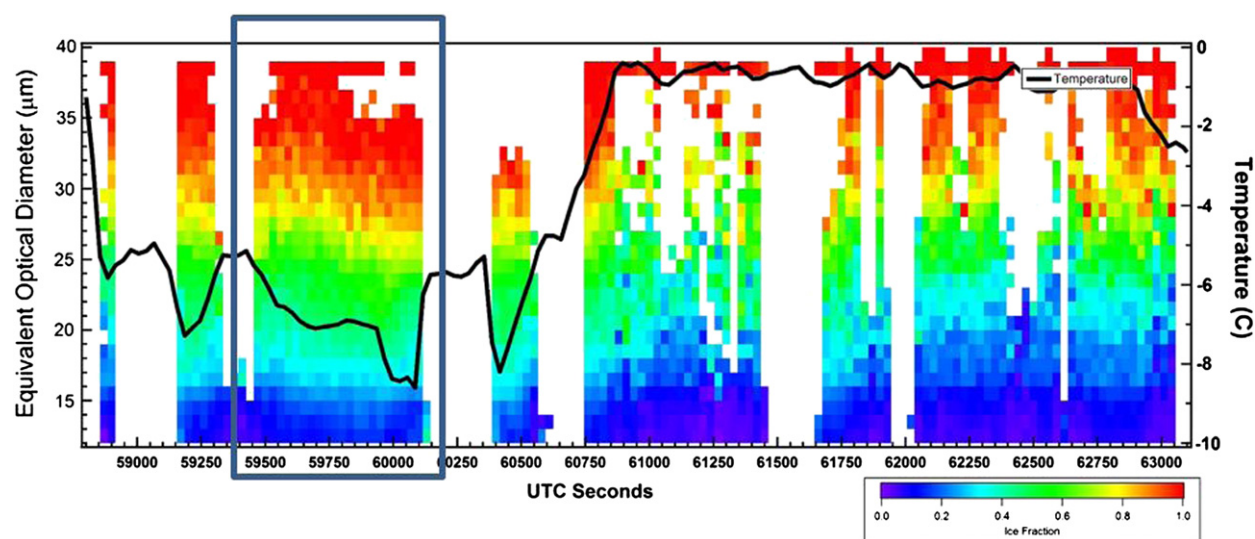


Fig. 11. In this contoured time series, the color coding represents the ice fraction as a function of equivalent optical diameter. Also shown is the temperature (black curve). The box highlights the region where it can be seen that the ice fraction is increasing in the smaller sizes.

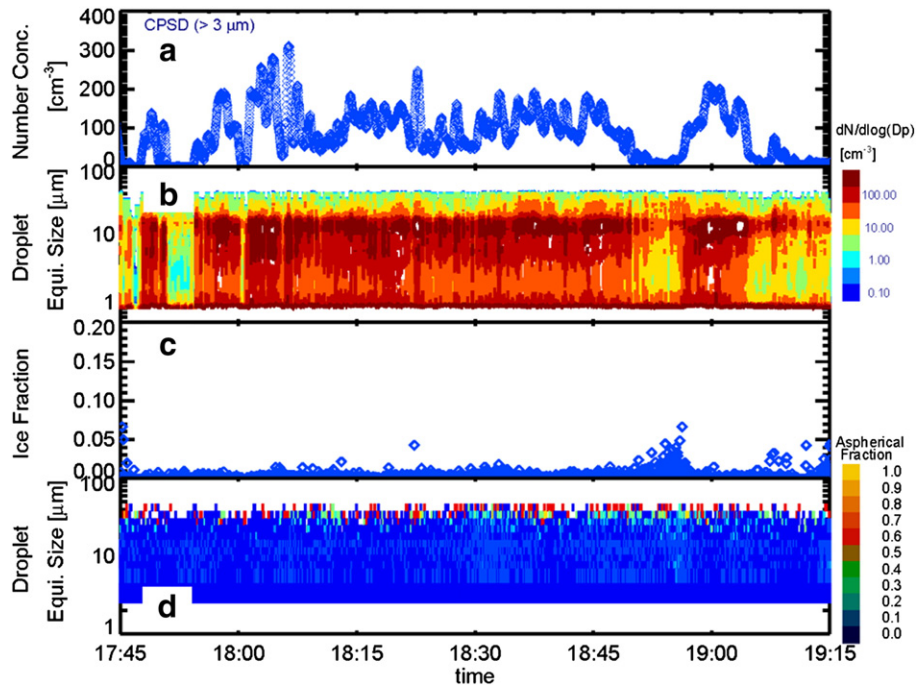


Fig. 12. These time series of measurements made during the occurrence of a mixed phase cloud show an example of (a) the CPSPD total number concentration and ice fraction, (b) the size distributions of number concentration, (c) the average ice fraction over all sizes and (d) the ice fraction as a function of optical equivalent diameter.

3.3. Discussion

Before proceeding with additional commentary relating some of the cloud processes to the observations that have been presented above, it is emphasized that these are preliminary results from a narrow range of conditions and that the airborne observations were made during instrument evaluation flights with no scientific objectives. All of the following conjectures about the observations are meant to incite questions rather than offer answers to the trends in the ice fractions that were seen in the data. These preliminary results are also meant to illustrate the capabilities of the instrument and highlight its potential as a potent tool for unraveling the difficult questions that still remain about ice formation and evolution in cloud.

In Figs. 10c and 11 the ice fraction gradually increases as the aircraft proceeds from the cloud edge to the interior and ambient temperature decreases. Given that the average ice fraction is taken over all detected particles, if we assume for the moment that this cloud is a mixture of water droplets and ice crystals, then the increasing ice fraction implies that the number of ice crystals with respect to water droplets is increasing. This change from liquid water to ice is a measure of the amount of glaciation through the section of cloud sampled. Given that we expect the rate of glaciation to be a function of the temperature, it is intuitively satisfying to see that the ice fraction increases as the temperature decreases from -7°C to -9°C .

The size distributions of the ice fraction in Fig. 11 show that they are highest in the largest particles, with the smaller particle ice fractions increasing as the temperature decreases. Laboratory studies have demonstrated that larger droplets

freeze before smaller ones (Gonda and Yamazaki, 1984) and that when droplets freeze, they can remain spherical for up to 20 min before evolving into aspherical shapes. Hence, the evolution of the ice fraction with size and temperature may also be related to the age of the cloud.

The results from the mountaintop experiment are intriguing given the average temperature that hovers near freezing yet during various periods up to 40% of the cloud particles in the size range of the CPSPD are ice. This variability is likely a result of cloud particles that are either falling from colder regions above or are being advected from their source region upwind, such that the local temperature is not representative of the air mass where the particles were formed, and blowing snow from the surface cannot be discounted. Nevertheless, the presence of high fractions of ice when local temperatures should be promoting melting or sublimation is an interesting phenomenon that needs further investigation.

4. Summary

In conclusion we have presented a new instrument that implements the measurement of single particle light scattering with polarization to extract information about the water phase of particles in cloud. Its primary advantage over its predecessor, the CAS-POL, is the modification of extended arms that hold the optical components so that their tips have the “Korolev” design that forces shattered particles away from the sample volume. This paper, illustrates the potential of this technique for distinguishing liquid water from ice and

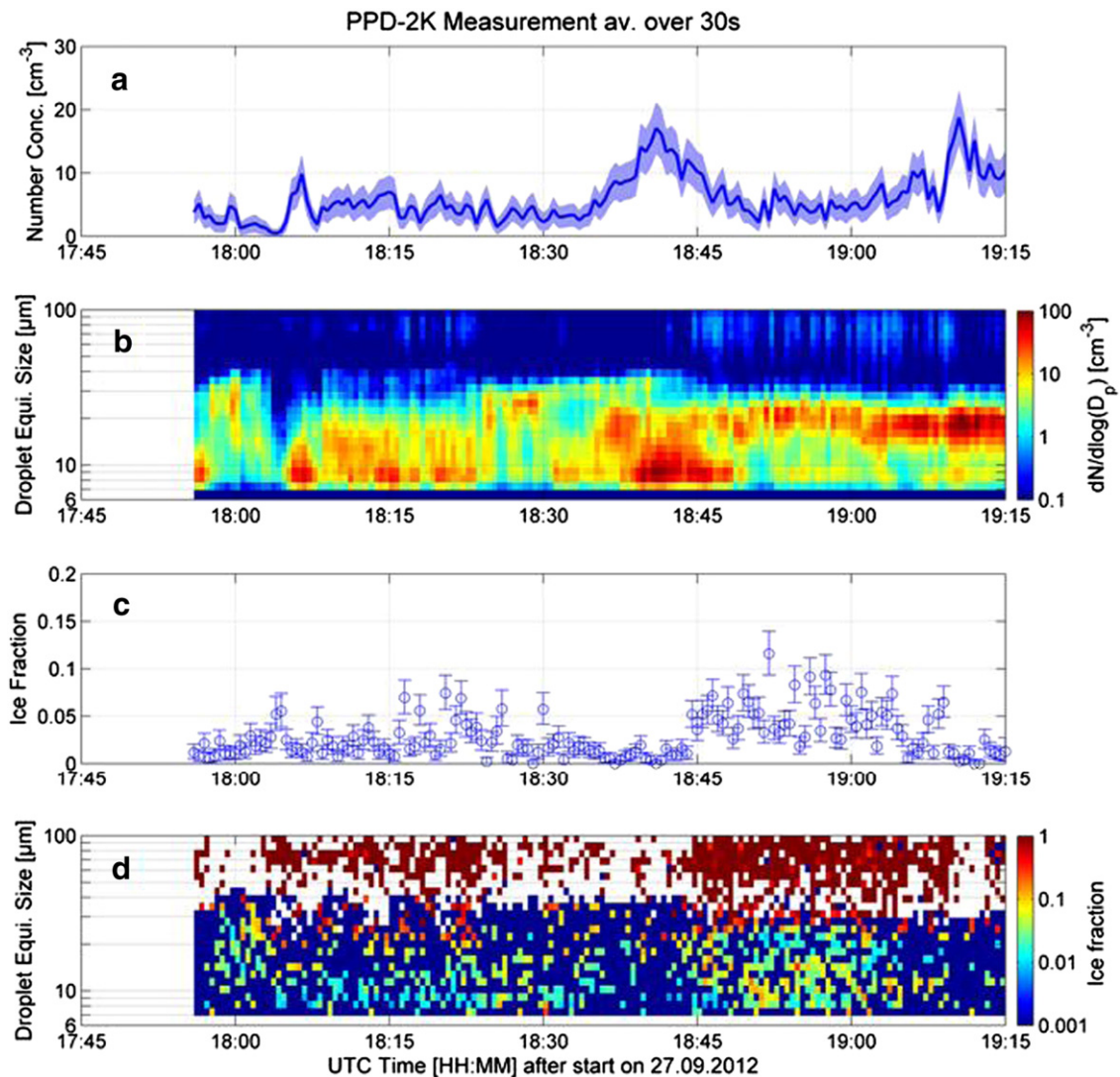


Fig. 13. These time series, similar to those shown in Fig. 12, illustrate an example of the PPD2-K (a) number concentration with a 1 Sigma Uncertainty contour, (b) the size distribution (c) and (d) the ice fraction based on the image analysis. These data correspond to the time period encompassed in Fig. 12.

for helping us finally resolve some of nature's riddles related to ice processes in cloud.

Acknowledgments

The authors would like to thank Mike Poellot and David Delene of the University of North Dakota for aircraft flight support, Bill Dawson of Droplet Measurement Technologies for calibration and maintenance of the CPSPD, Alexei Korolev of Environment Canada for his Probe tip design, Armin Afchine of Forschungszentrum Jülich for Airflow Modeling, Martina Krämer and Forschungszentrum Jülich for providing funding to develop the CPSPD and Kaare Anderson of the Goodrich Corporation for flight hour donation. We would also like to thank Dagmar Rosenow, University of Leipzig, for organizing the field project at the Zugspitze and making possible the deployment of the CPSPD during that project.

References

- Baumgardner, D., 1986. A new technique for the study of cloud microstructure. *J. Atmos. Ocean. Technol.* 3, 340–343.
- Baumgardner, D., Strapp, W., Dye, J.E., 1985. Evaluation of the forward scattering spectrometer probe. Part II: corrections for coincidence and dead-time losses. *J. Atmos. Ocean. Technol.* 2, 626–632.
- Baumgardner, D., et al., 2001. The cloud, aerosol and precipitation spectrometer (CAPS): a new instrument for cloud investigations. *Atmos. Res.* 59–60, 251–264.
- Baumgardner, D., et al., 2005. The shapes of very small cirrus particles derived from in situ measurements. *Geophys. Res. Lett.* 32, L01806. <http://dx.doi.org/10.1029/2004GL021300>.
- Baumgardner, D., et al., 2011. Airborne instruments to measure atmospheric aerosol particles, clouds and radiation: a cook's tour of mature and emerging technology. *Atmos. Res.* 102, 10–29. <http://dx.doi.org/10.1016/j.atmosres.2011.06.021>.
- Baumgardner, D., et al., 2012. In situ, airborne instrumentation: addressing and solving measurement problems in ice clouds. *Bull. Am. Meteorol. Soc.* 29–34.
- Bohren, C.F., Huffman, D.R., 1983. Absorption and scattering of light by small particles. John Wiley & Sons, Inc.(544 pp.).
- Bundke, U., et al., 2008. The fast ice nucleus chamber FINCH. *Atmos. Res.* 90, 180–186.

- Cotton, R., et al., 2009. The ability of the small ice detector (SID-2) to characterize cloud particle and aerosol morphologies obtained during flights of the FAAM BAe-146 research aircraft. *J. Atmos. Ocean. Technol.* 27, 290–303.
- Field, P.R., et al., 2003. Ice particle interarrival times measured with a Fast FSSP. *J. Atmos. Ocean. Technol.* 20, 249–261.
- Field, P.R., et al., 2006. Shattering and particle interarrival times measured by optical array probes in ice clouds. *J. Atmos. Ocean. Technol.* 23, 1357–1370.
- Fugal, J.P., Shaw, R.A., 2009. Cloud particle size distributions measured with an airborne digital in-line holographic instrument. *Atmos. Meas. Tech.* 2, 259–271.
- Fugal, J.P., et al., 2004. Airborne digital holographic system for cloud particle measurements. *Appl. Opt.* 43, 5987–5995.
- Fugal, J.P., et al., 2009. Practical methods for automated reconstruction and characterization of particles in digital in-line holograms. *Meas. Sci. Technol.* 20, 075501. <http://dx.doi.org/10.1088/0957-0233/20/7/075501>.
- Fukuta, N., Kramer, G.K., 1968. A fast activation continuous ice nuclei counter. *J. Rech. Atmosph.* 3, 169–173.
- Glen, A., Brooks, S.D., 2013. A new method for measuring optical scattering properties of atmospherically relevant dusts using the Cloud and Aerosol Spectrometer with Polarization (CASPOL). *Atmos. Chem. Phys.* 13, 1345–1356. <http://dx.doi.org/10.5194/acp-13-1345-2013>.
- Gonda, Yamazaki, T., 1984. Initial growth forms of snow ice crystals growing from frozen cloud droplets. *J. Meteorol. Soc. Jpn.* 62, 190–192.
- Harris-Hobbs, R.L., Cooper, W.A., 1987. Field evidence supporting quantitative predictions of secondary ice production rates. *J. Atmos. Sci.* 44, 1071–1082.
- Johnson, A., et al., 2014. Detection and quantification of ice with the Small Ice Detector 2 HIAPER (SID-2H). *J. Atmos. Ocean. Technol.* (in press).
- Kaye, P., et al., 2008. Classifying atmospheric ice crystals by spatial light scattering. *Opt. Lett.* 33, 1545.
- Knollenberg, R.G., 1976. Three new instruments for cloud physics measurements: the 2-D spectrometer probe, the forward scattering spectrometer probe and the active scattering aerosol spectrometer. *Amer. Met. Society, Int'l Conf. on Cloud Physics*, pp. 554–561.
- Knollenberg, R.G., 1981. Techniques for probing cloud microstructure. In: Hobbs, P.V., Deepak, A. (Eds.), *Clouds, Their Formation, Optical Properties and Effects*. Academic Press (495 pp.).
- Korolev, A.V., Isaac, G.A., 2003. Roundness and aspect ratio of particles in ice clouds. *J. Atmos. Sci.* 60, 1795–1808.
- Korolev, Alexei, Emery, Edward, Creelman, Kirk, 2013. Modification and Tests of Particle Probe Tips to Mitigate Effects of Ice Shattering. *J. Atmos. Oceanic Technol.* 30, 690–708.
- Lance, S., et al., 2010. Water droplet calibration of the Cloud Droplet Probe (CDP) and in-flight performance in liquid, ice and mixed-phase clouds during ARCPAC. *Atmos. Meas. Tech.* 3, 1683–1706.
- Mie, G., 1908. Beiträge zur Optik trüber Medien, speziell kolloidaler Metallösungen. *Ann. Phys.* 25, 377–445.
- Mishchenko, M.I., 2000. Calculation of the amplitude matrix for a nonspherical particle in a fixed orientation. *Appl. Opt.* 39, 1026–1031.
- Nicolet, M., et al., 2007. Depolarization ratios of singles ice particles assuming finite circular cylinders. *Appl. Opt.* 46, 4465–4476.
- Nicolet, M., et al., 2010. Single ice crystal measurements during nucleation experiments with the depolarization detector IODE. *Atmos. Chem. Phys.* 10, 313–325. <http://dx.doi.org/10.5194/acp-10-313-2010>.
- Nicolet, M., Schnaiter, M., Stetzer, O., 2012. Circular depolarization ratios of single water droplets and finite ice circular cylinders: a modeling study. *Atmos. Chem. Phys.* 12, 4207–4214. <http://dx.doi.org/10.5194/acp-12-4207-2012>.
- Schnaiter, M., et al., 2012. Influence of particle size and shape on the backscattering linear depolarisation ratio of small ice crystals – cloud chamber measurements in the context of contrail and cirrus microphysics. *Atmos. Chem. Phys.* 12, 10465–10484. <http://dx.doi.org/10.5194/acp-12-10465-2012>.
- Turner, F.M., Radke, L.F., 1973. The design and evaluation of an airborne optical ice particle counter. *J. Appl. Meteorol.* 12, 1309–1318.
- Ulanowski, Z., Kaye, P.H., Hirst, E., Greenaway, R.S., Cotton, R.J., Hesse, E., Collier, C.T., 2013. Incidence of rough and irregular atmospheric ice particles from Small Ice Detector 3 measurements. *Atmos. Chem. Phys. Discuss.* 13, 24975–25012. <http://dx.doi.org/10.5194/acpd-13-24975-2013>.
- Weickman, H., 1945. Formen und Bildung atmosphärischer Eiskristalle. *Beitr. Phys. Atmos.* 12–52.
- Wendisch, M., Brenguier, J.-L. (Eds.), 2013. *Airborne measurements for environmental research: methods and instruments*. Wiley-VCH Verlag GmbH & Co. KGaA, Weinheim, Germany. ISBN: 978-3-527-40996-9 (655 pp.).
- Wendisch, M., Keil, A., Korolev, A.V., 1996. FSSP characterization with monodisperse water droplets. *J. Atmos. Ocean. Technol.* 13, 1152–1165.